Dynamic decoupling in the presence of colored control noise

Ido Almog,[1] Gil Loewenthal,[1] Jonathan Coslovsky,[1] Yoav Sagi,[2] and Nir Davidson[1]
[1]*Department of Physics of Complex Systems, Weizmann Institute of Science, Rehovot 76100, Israel*
[2]*JILA, National Institute of Standards and Technology and University of Colorado, Department of Physics, University of Colorado, Boulder, Colorado 80309-0440, USA*
(Received 30 March 2016; published 12 October 2016)

An optimal dynamic decoupling of a quantum system coupled to a noisy environment must take into account also the imperfections of the control pulses. We present a formalism which describes, in a closed-form expression, the evolution of the system, including the spectral function of both the environment and control noise. We show that by measuring these spectral functions, our expression can be used to optimize the decoupling pulse sequence. We demonstrate this approach with an ensemble of optically trapped ultracold rubidium atoms, and use quantum process tomography to identify the effect of the environment and control noise. Our approach is applicable and important for any realistic implementation of quantum information processing.

DOI: 10.1103/PhysRevA.94.042317

I. INTRODUCTION

The paradigm of a two-level system (TLS) is central to quantum information (QI), where it is applied as a quantum bit (qubit), the building block for information transfer, quantum memory, or the computational gates. Coupling to a noisy environment, which is inherent to any system, reduces the purity of the TLS, and thus limits its usefulness for any QI application. Several techniques have been developed to increase the quality of the quantum operation of the TLS, which is usually quantified by a measure called fidelity [1].

One of these techniques is dynamic decoupling (DD), where a pulsed control field is used to couple the two levels of the TLS, and thus reduce their coupling to the environment [2]. In QI, DD is used mainly to reduce the decay of the fidelity of a TLS, making it useful for longer times, as demonstrated in a large variety of systems [3–10]. It was theoretically and experimentally shown that the success of these schemes can be predicted using a measurable spectral function that describes the coupling of the system to the environment, sometimes referred to as the "bath spectrum" [10–19]. In all of these proposals, higher rates of the control pulses generate better decoupling from the environment. However, in any realistic implementation there are imperfections in the control field, hence dynamic decoupling sequences become increasingly ineffective as the number of pulses grows.

In the quest for robust DD in the presence of pulse imperfections, it is usually assumed that errors in the control pulses are uncorrelated [20–23]. This "white" noise assumption is commonly used when estimating the fidelity of a gate by applying the same gate again and again many times but in a random manner, an approach known as "benchmarking" [24]. In contrast to this assumption, as we show below, the control pulses often have correlated errors leading to a colored nonflat spectral function, which must be taken into account. Although the bath-system approach can be used to calculate the system-environment coupling for realistic and robust pulse sequences [25–28], it is still not possible to get their outcome fidelity without a unified spectral treatment taking into account both the spectral noises in the environment and a spectral description of the (classical) noise of the control.

In this work, we study the combined effect of coupling to the environment and a DD control field with colored noise on a TLS, and develop a closed-form expression to describe it by the two corresponding spectral functions. We measure these spectral functions with an ensemble of ultracold optically trapped ^{87}Rb atoms, and then use them to predict the outcome of a generic DD scheme and its overall fidelity. Using quantum process tomography [1,4], we show and explain the effect of each of the spectral functions with any initial state.

II. SYSTEM SUBJECTED TO REALISTIC DYNAMIC DECOUPLING

We consider a general TLS model with energy fluctuations and a noisy control field, described by the effective Hamiltonian

$$\hat{H} = \frac{\hbar}{2}[\omega_0 + \delta(t)]\sigma_z + \frac{\hbar}{2}[\Omega(t)e^{-i\omega_0 t}\sigma_x + \text{H.c.}]. \quad (1)$$

Here, ω_0 is the transition frequency between the two states and $\Omega(t)e^{-i\omega_0 t}$ is a noisy (classical) external control field, which is used for the DD. The operators σ_i are the Pauli matrices, written in the two-level basis denoted by $|2\rangle$ and $|1\rangle$. The noise in the control field enters through $\Omega(t) = \Omega_0(t)[1 + n_c(t)]$, where $\Omega_0(t)$ is the desired, noiseless control. The frequency detuning noise, $\delta(t)$, and the control noise, $n_c(t)$, are random functions in time, with a mean value of zero. Our analysis can be readily extended for control fields having both multiplicative and additive noise, multiaxis pulses, and frequency and phase noise in the control.

The short time evolution of an initial state can be described by the reduced density matrix $\tilde{\rho} = \frac{1}{2}(\rho_x\sigma_x + \rho_y\sigma_y + \rho_z\sigma_z + \mathbf{I})$, to second order in the noises (see the Appendix). In the interaction picture of $H_0(t) = \hbar\sigma_x\Omega_0(t)/2 + \hbar\sigma_z\omega_0/2$, and under the weak coupling assumption [14], the effective Hamiltonian, $\tilde{H}_{\text{int}}(t) = \hbar\delta(t)\frac{\sigma_z}{2}\cos\left(\int_0^t d\tau\Omega_0(\tau)/2\right) + \hbar n_c(t)\Omega_0(t)\frac{\sigma_x}{2}$, can be considered as a perturbation. The master equation for the density matrix operator is

$$\dot{\tilde{\rho}}(t) = \left\langle \frac{1}{(i\hbar)^2}\int_0^t dt_2\left[\tilde{H}_{\text{int}}(t), \tilde{H}_{\text{int}}(t_2)\tilde{\rho}(t)\right] + \text{H.c.}\right\rangle, \quad (2)$$

where $\langle\cdots\rangle$ stands for expectation value, after tracing out the environment. The two-term interaction Hamiltonian plugged into Eq. (2) gives rise to four terms, which are integrated over

time T to find the short-time evolution of the density matrix. The outcome is the paper's theoretical main result

$$\Delta\rho(T) = \int_{-\infty}^{\infty} df \left[\underbrace{-\frac{\rho_x\sigma_x + \rho_y\sigma_y}{4} G_\delta(f)F_\delta(f)}_{\text{coupling to the environment}} \underbrace{-\frac{\rho_y\sigma_y + \rho_z\sigma_z}{4} G_c(f)F_c(f)}_{\text{noise in the control}} + \underbrace{\left(\frac{\rho_z\sigma_x}{4} G_{\delta c}(f) + \frac{\rho_x\sigma_z}{4} G_{c\delta}(f)\right)F_{\delta c}(f)}_{\text{cross-correlation between environment and control}} \right]. \quad (3)$$

The three spectral overlap integrals in Eq. (3), determine the full evolution of the density matrix. They describe the effect of the coupling to the environment, the noise in the control field, and cross-correlation between the environment and the control field, respectively. The first term is similar to the spectral overlap integral of Refs. [11,14,17].

The two bath spectral functions $G_\delta(f)$ and $G_c(f)$ describe the correlation at different times of the environment and the noise of the control

$$\begin{aligned} G_\delta(f) &\equiv \int_{-\infty}^{\infty} e^{-2\pi i f\tau} \langle \delta(t)\delta(t+\tau)\rangle d\tau, \\ G_c(f) &\equiv \int_{-\infty}^{\infty} e^{-2\pi i f\tau} \langle n_c(t)n_c(t+\tau)\rangle d\tau. \end{aligned} \quad (4)$$

The filter spectral functions $F_\delta(f)$ and $F_c(f)$ encapsulate the information regarding the modulation done by the control, during the time period T, and are written explicitly for sequences composed of π_x or π_{-x} pulses as

$$\begin{aligned} F_\delta(f) &\equiv \left| \int_0^T dt\, e^{-2\pi i f t} \cos\left(\int_0^t \Omega_0(\tau) d\tau \right) \right|^2, \\ F_c(f) &\equiv \left| \int_0^T dt\, e^{-2\pi i f t} \Omega_0(t) \right|^2. \end{aligned} \quad (5)$$

Similarly, $F_{\delta c}(f)$, $G_{\delta c}(f)$, and $G_{c\delta}(f)$, describing the cross-correlations between the control noise, $n_c(t)$, and the environment noise, $\delta(t)$, are given in the Appendix, but are negligible in our experiment.

Inverting the relation in Eq. (3), in order to find the bath spectral functions from time evolution measurements of the density matrix is hard, when two or more overlap integrals are involved. However, it is possible to reduce these expressions to a single overlap integral by choosing wisely the initial state and DD sequence, essentially separating the problems of finding the two spectral functions. For example, in order to find the environment bath spectrum, $G_\delta(f)$, we have used a random initial state and employed envelope spectroscopy which is insensitive to the control noise. With this choice, the evolution of the reduced density matrix, as given in Eq. 3, depends only on a single overlap integral [14]. By using a filter function that consists of several discrete peaks, which samples the environment bath spectrum at these discrete frequencies, one can invert the spectral overlap integral by solving a set of linear equations [10] or a single linear equation in the case of a single peak filter function [14].

Similarly, in order to measure the control noise spectral function, $G_c(f)$, it is worthwhile to eliminate the overlap integral of the environment. This is done by applying a π-pulse sequence starting with an ensemble initialized to the state $\rho(0) = |1\rangle$. Since this essentially keeps the system in states $|1\rangle$ and $|2\rangle$, which are insensitive to the pure dephasing environment noise, Eq. (3) reduces to (see Appendix) $\Delta\rho(T) = \frac{1}{4}\langle\rho_y^2(T)\rangle\sigma_z$, with

$$\left\langle \rho_y^2(T) \right\rangle = \int_{-\infty}^{\infty} df\, G_c(f)F_c(f). \quad (6)$$

By applying a $\pi/2$ pulse followed by state detection, we can measure $\langle\rho_y^2(T)\rangle$, which is sensitive to the overlap integral, as explained.

III. MEASUREMENT OF THE CONTROL NOISE SPECTRUM

Our experimental setup is described in [29]. In short, about 2.5×10^5 ultracold ^{87}Rb atoms are confined in an external optical potential created by two 1.06 μm crossed laser beams. The temperature of the atomic ensemble is 1.7 μK, with a peak density of 2×10^{13} cm^{-3}. The two metastable states $|1\rangle \equiv |F = 1, m = -1\rangle$ and $|2\rangle \equiv |F = 2, m = +1\rangle$ of the $5^2S_{1/2}$ manifold are chosen as the TLS. The energy difference between these states is, to first order, magnetically insensitive, at the applied magnetic field of 3.2 G [30]. The control field is implemented using a two-photon microwave (MW) and radio frequency (RF) transition detuned by $\Delta \approx 110$ kHz from the intermediate $|F = 2, m = 0\rangle$ level, taking into account all energy shifts (differential AC Stark shift, second-order magnetic shifts, mean-field interaction and MW dressing). We measure the state of the atoms using a fluorescence detection scheme [4].

The main sources for the noises $\delta(t)$ and $n_c(t)$ are well understood in our system. The environment noise, $\delta(t)$, is due to the differential AC Stark shift of elastically colliding atoms in the optical dipole trap [4]. For each of the atoms, the environment is the atomic ensemble itself, randomizing the atomic trajectory after every elastic collision. The noise in the control is mostly due to magnetic fluctuations. The magnetic noise enters through the single-photon detuning of the two-photon transition, $\Delta(t)$, which is magnetically sensitive to first order. This fluctuating detuning changes the effective Rabi frequency of the two-photon transition,

$$\Omega(t) = \Omega_1\Omega_2/2\Delta(t), \quad (7)$$

where Ω_1 and Ω_2, the single photon Rabi frequencies of the MW and RF fields, are essentially noiseless in our system. Note that, since the two states of the TLS are magnetically insensitive, noise in the magnetic field affects only the control field, hence the cross-correlation term in Eq. (3), is negligible. We expect to find a dominant contribution to the noise at 50 Hz and higher harmonics, arising from the electrical grid.

Figure 1(a) presents the measured variance, $\langle\rho_y^2\rangle$, versus the pulse rate for 40 pulses of CPMG-4 DD sequence. The sequence CPMG-n, initially introduced by Carr, Pur-

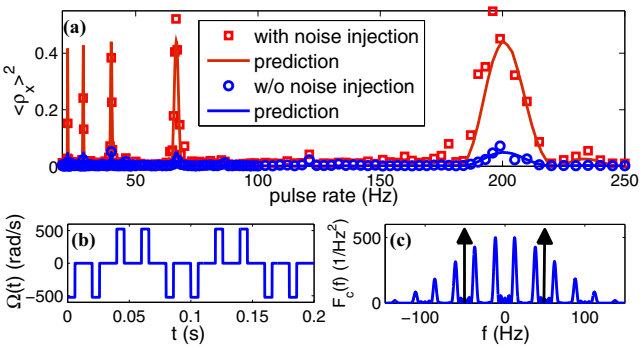

FIG. 1. The control noise spectrum. (a) The square (circle) data set is the measured $\langle\rho_y^2\rangle$ after 40 pulses of CPMG-4, with (without) a 4 mG peak-to-peak magnetic noise injected at a frequency of 50 Hz. The solid lines are calculated from Eqs. (6) and (7), with an independent measurement of the magnetic noise. (b),(c) The filter function $F_c(f)$ of a CPMG-4 sequence with pulse rates of (b) 50 Hz and (c) 67 Hz. The arrows represent the 50 Hz component of the noise, which have significant overlap with the peaks of the filter function only for the sequence with a pulse rate of 67 Hz (c). The inset shows an illustration of a CPMG-4 control field at a pulse rate of 67 Hz. Negative pulses represent a π phase shift of the control field. (the duration of the pulses is not to scale). Points A, B, C, and D are defined in the text.

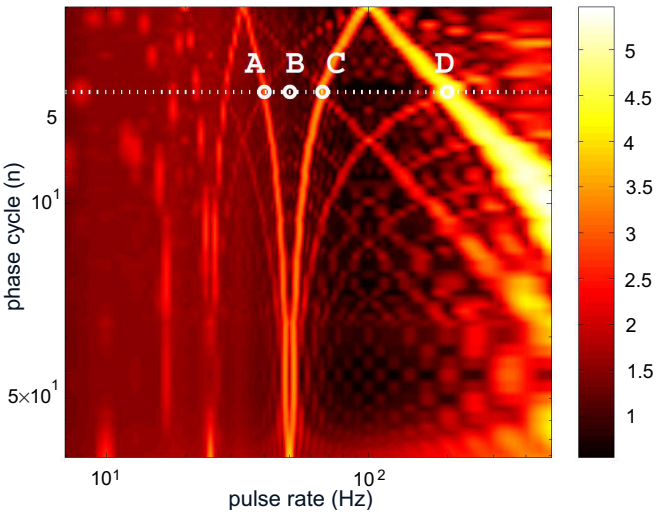

FIG. 2. A two-dimensional map of the predicted logarithm of fidelity decay rate (in units of s^{-1}) as a function of the pulse rate f_{DD} and phase cycle n of the CPMG-n pulse sequence without the injection of noise at 50 Hz. The brightness (color online) represents the decay rate of the fidelity in logarithmic scale (black represents no decay). Points A, B, C, and D are defined in the text. The dashed line correspond to $n = 4$ (i.e., CPMG-4 sequence).

cell, Meiboom, and Gill [31,32], is composed of equally spaced π pulses with a phase alternating between π and $-\pi$ after every $n/2$ pulses. We repeat the measurements with and without deliberately injecting a 50 Hz magnetic noise (by driving a current in a nearby coil, phase locked to the electrical grid) to further increase the control noise.

The measured spectrum is reproduced by using our control noise spectrum, which consists of a discrete peak at 50 Hz, a DC component, and a small component of white noise. Notice that since the filter function of CPMG-4 at pulse rate of 50 Hz has no peak at this frequency, there is no special feature around 50 Hz, as illustrated in Fig. 1(b). This is in contrast to a pulse rate of 67 Hz which overlaps a peak of the control noise, as shown in Fig. 1(c). Using Eqs. (5)–(7) and a direct independent measurement of the 50 Hz magnetic noise, we depict the calculated control noise spectrum [in Fig. 1(a)], showing discrete peaks at frequencies of $200/(2m-1)$ Hz, with $m = 1,2,\ldots,$ in excellent agreement with the measured noise spectrum without any fit parameter. The entire spectrum has a small bias which is due to imperfections in the state detection and uncorrelated (white) noise in the control pulses. The latter is measured separately using a higher number of pulses (100), to increase the sensitivity. Finally, a DC control noise of 3×10^{-5} is measured using a CPMG DD sequence (with no phase alternation), whose filter function has a prominent component at DC.

By choosing one of the peaks in the spectrum of Fig. 1(a) and repeatedly measuring its noise component, we were able to reduce it by about 50% by injecting a 50 Hz component to a nearby coil and searching for the phase and amplitude which minimize the peak.

IV. DYNAMIC DECOUPLING SEQUENCE ENGINEERING

The usefulness of Eq. (3) stems from its ability to predict the performance of any DD sequence, given that the two spectral functions, $G_\delta(f)$ and $G_c(f)$, are known. For the purpose of optimizing the DD we quantify its success with the fidelity, defined by $\mathcal{F} = \mathrm{Tr}\{\rho(t)\rho(0)\}$, as it includes both the effects of pulse imperfection and the coupling to the environment. The short time fidelity [neglecting the last term in Eq. (3)] can be written (see the Appendix) as

$$\mathcal{F} = 1 - \frac{\rho_x^2+\rho_y^2}{4}\int_{-\infty}^{\infty} df\, G_\delta(f)F_\delta(f) - \frac{\rho_y^2+\rho_z^2}{4}\int_{-\infty}^{\infty} df\, G_c(f)F_c(f). \quad (8)$$

It is helpful to plot the decay rate of the fidelity as a function of the pulse sequence parameters. In such a plot, it is easy to graphically identify the region in parameter space where the performance of the DD sequence is optimized. These plots can be reproduced for any dynamic decoupling sequence and noise spectrum, as is demonstrated here for CPMG and Uhrig [9] sequences.

In the case of CPMG-n, the natural choice of parametrization is the pulse rate f_{DD} and the parameter n. An example of such a map, based on the two measured spectral bath functions of our system, is presented in Fig. 2, calculated for the worst case fidelity (taking an initial state of $\rho_y = 1$). The regions with the highest fidelity are clearly visible.

Although the map exhibits some complex features, the central ones can be qualitatively understood. At low control pulse rates, the fidelity decay rate follows a Lorentzian, reflecting the Poisson statistics of the cold atomic collisions [4]. At higher pulse rates, there is a reduction in fidelity caused

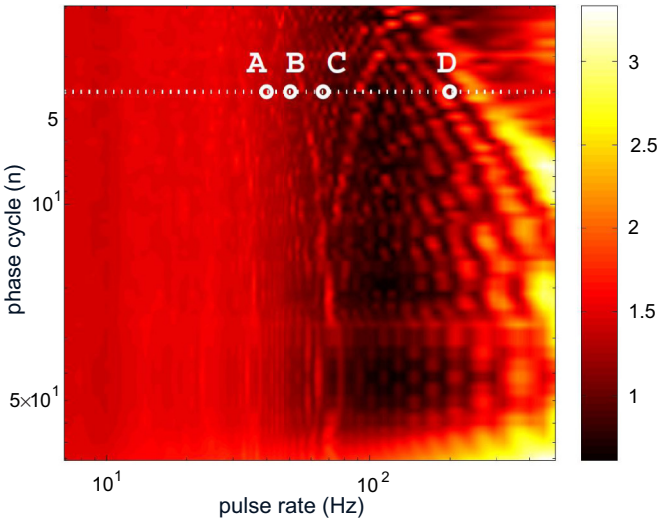

FIG. 3. The predicted logarithm of of the fidelity decay rate (in units of s^{-1}) as a function of the average pulse rate f_{DD} and the phase cycle n, for a Uhrig-n pulse sequence. The plot was calculated for a 20 π-pulse sequence, without the noise injection at 50 Hz. Using the previously defined point A, B, C, and D for reference with the CPMG map, we note that the high decay rate features are different.

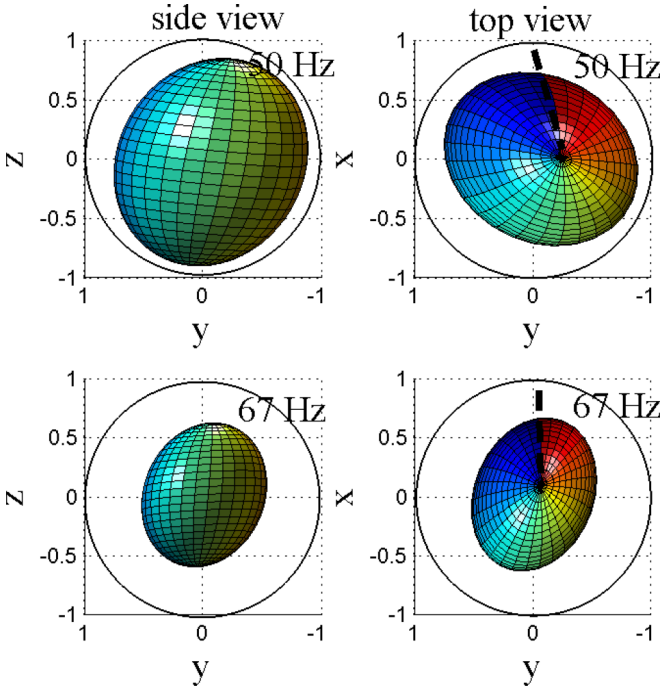

FIG. 4. Process tomography of CPMG-4 DD scheme in the presence of a noisy control field. A color code representing the state phase and a dotted line representing the zero phase states are used to indicate the rotations around the z axis. Outer and inner spheres represent initial and final states, respectively. Top: measured Bloch sphere after 50 pulses at a rate of 50 Hz and with a 4 mG magnetic noise injection. Top and side view are shown on the right and left sides, respectively. Bottom: same measurement but with a pulse rate of 67 Hz. The different axes suffer from different decay rates, as expected from Eq. (3). For our π_x-pulse sequence, the x axis decay is slower.

by the white noise component of the control field and arising from the large number of pulses. Large-n cycles are also less successful, since their filter function has a large spectral component at DC, sampling the slow drifts in the strength of the control field. The control noise, originating mainly from the 50 Hz magnetic noise, produces a dominant feature appearing as strips on the map. The points A–D correspond to the points marked in Fig. 1.

Clearly the same procedure can be applied for any DD pulse sequence and is not restricted to equally spaced pulses. As an example, in Fig. 3 we present the expected decay rate of our system for a Uhrig-n pulse sequence [9], where n is the phase cycle and has the same meaning as in the CPMG-n sequences. Comparing between the maps for Uhrig-n and CPMG-n, it can be seen that the features of the 50 Hz control noise are still present but have become "shattered."

V. COHERENCE OF AN ARBITRARY INITIAL STATE

Process tomography [1] is a technique used to characterize the TLS state after being manipulated by the control (referred here by *process*), for any initial state. A great advantage of the formalism presented in Eq. (3) is that it predicts the entire three-dimensional effect of the process on the system, which is simply visualized as a deformed sphere in the Bloch representation.

For process tomography we repeat the process with four initial states, $\rho(0) = \frac{1}{2}(\Sigma + \mathbf{1})$, where Σ is one of the Pauli matrices σ_z, $-\sigma_z$, σ_x, and σ_y. For each initial state, the final state is measured by applying six different control pulses, followed by a state detection. For a linear process, this information is sufficient to construct the process matrix [1,4].

The results of the process tomography measurements are shown in Fig. 4, for two DD processes: CPMG-4 at 50 and 67 Hz pulse rates, corresponding to points B and C in Fig. 2. Although close in frequency, the two processes differ significantly, in agreement with our measured bath spectral functions. For the 50 Hz process, there is no dominant control noise (as explained before), hence the decay is mostly due to the coupling to the environment. The decay of the z axis is the lowest, limited by a T_1 process (not included in our model, measured to be ≈ 5 sec). The decay of the other two axes is similar, which is expected from Eq. (3), since the coefficients ρ_x and ρ_y appear symmetrically in the terms describing the coupling to the environment. In contrast, in the 67 Hz process, the decay in the y and z axes is faster since it is also affected by the noise in the control (involving the coefficients ρ_x and ρ_y).

VI. CONCLUSIONS

The formalism developed here together with the one described in [14] gives a recipe for designing a DD sequence: First measure the spectral function defining the coupling to environment. Then measure the spectral function that characterizes the noise in the control field. Choose a general DD sequence parametrized by few parameters. Use the overlap integrals to calculate the performance map as a function of these parameters. Choose high fidelity regions for the DD sequences.

Generally, any realistic control has a colored noise spectrum with different frequency components: Microwave transitions have frequency components related to the electricity grid, optical transitions have mechanical frequencies of the optical elements [33], and trapped atoms or ions have frequencies related to their oscillation [34]. Although the the optimal pulse is system dependent, the most efficient way to find it is general, as we have shown here.

ACKNOWLEDGMENTS

We acknowledge the financial support of MINERVA, ISF, and DIP.

APPENDIX

1. Equation of motion for system density operator

a. Mathematical derivation

We are interested in the short time evolution of the system density operator determined by the Hamiltonian

$$\hat{H} = \frac{\hbar}{2}[\omega_0 + \delta(t)]\sigma_z + \frac{\hbar}{2}[\Omega(t)e^{-i\omega_0 t}\sigma_x + \text{H.c.}]. \tag{A1}$$

Using the notation $\Omega(t) = \Omega_0(t)[1 + n_c(t)]$, we separate the desired control field, $\Omega_0(t)$, from the noisy term, $n_c(t)$, and define the (noiseless) action

$$\vartheta(t) = \int_0^t d\tau\, \Omega_0(\tau)/2. \tag{A2}$$

It is convenient to move to the interaction picture of $H_0(t) = \hbar\sigma_x\Omega_0(t)/2 + \hbar\sigma_z\omega_0/2$. In this picture, when the change in the system density operator during the bath correlation time is negligible, the effective Hamiltonian, $\tilde{H}_{\text{int}}$, can be considered as a perturbation. This assumption, called the *weak coupling* assumption, is naturally valid in QI since the quantum gate or memory is not useful when the decay of coherence is not small during its time of operation. In this case, the system's density operator obeys the following master equation (to second order in the noise):

$$\dot{\tilde{\rho}}(t) = \left\langle \frac{1}{(i\hbar)^2}\int_0^t dt_2[\tilde{H}_{\text{int}}(t),[\tilde{H}_{\text{int}}(t_2),\tilde{\rho}(t)]]\right\rangle, \tag{A3}$$

where $\langle\cdots\rangle$ stands for expectation value, coming from tracing out the environment.

The interaction Hamiltonian can be written explicitly as $\tilde{H}_{\text{int}}(t) = \hbar\delta(t)\tilde{S}_\delta(t) + \hbar n_c(t)\tilde{S}_c(t)$, with an operator related to the interaction with the environment

$$\begin{aligned}\tilde{S}_\delta(t) &= e^{i\sigma_x\int_0^t d\tau\Omega_0(\tau)/2}\frac{\sigma_z}{2}e^{-i\sigma_x\int_0^t d\tau\Omega_0(\tau)/2}\\ &= \frac{\sigma_z}{2}\cos[\vartheta(t)] + \frac{\sigma_y}{2}\sin[\vartheta(t)],\end{aligned} \tag{A4}$$

and an operator related to the noise in the control,

$$\begin{aligned}\tilde{S}_c(t) &= e^{i\sigma_x\int_0^t d\tau\Omega_0(\tau)/2}\frac{\Omega_0(t)\sigma_x}{2}e^{-i\sigma_x\int_0^t d\tau\Omega_0(\tau)/2}\\ &= \Omega_0(t)\frac{\sigma_x}{2}.\end{aligned} \tag{A5}$$

Plugging this into Eq. (A3), we get the equation for the density operator

$$\begin{aligned}\dot{\tilde{\rho}}(t) = &-\int_0^t dt_2\langle\delta(t)\delta(t_2)\rangle[\tilde{S}_\delta(t),[\tilde{S}_\delta(t_2),\tilde{\rho}(t)]]\\ &-\int_0^t dt_2\langle n_c(t)n_c(t_2)\rangle[\tilde{S}_c(t),[\tilde{S}_c(t_2),\tilde{\rho}(t)]]\\ &-\int_0^t dt_2\langle n_c(t)\delta(t_2)\rangle[\tilde{S}_c(t),[\tilde{S}_\delta(t_2),\tilde{\rho}(t)]]\\ &-\int_0^t dt_2\langle\delta(t)n_c(t_2)\rangle[\tilde{S}_\delta(t),[\tilde{S}_c(t_2),\tilde{\rho}(t)]].\end{aligned}$$

Three mechanisms, which are responsible for the density matrix evolution, can be identified in the four terms of the expression: The first term describes the effect of the environment, the second describes the effect of the noise of the control field and the last two are the result of the cross correlation between the control noise and the environment coupling.

Fortunately, each term in Eq. (A6) can be expressed as an overlap of two functions in the spectral domain. As all the derivations are similar and have a similar final result as the first two overlap integrals in the main text, we shall explicitly derive the spectral overlap integral expression for the two last cross-correlation terms. Starting from the fourth term, we plug Eqs. (A4) and (A5)

$$\begin{aligned}&-\int_0^t dt_2\langle\delta(t)n_c(t_2)\rangle[\tilde{S}_\delta(t),[\tilde{S}_c(t_2)\tilde{\rho}(t)]]\\ &=\int_0^t dt_2\langle\delta(t)n_c(t_2)\rangle\frac{1}{2}\sigma_x\Omega_0(t_2)\\ &\quad\times\{\rho_y(0)\sin[\vartheta(t)] + \rho_z(0)\cos[\vartheta(t)]\},\end{aligned}$$

and integrate to get the expression for the density matrix change due to this cross-correlation term

$$\begin{aligned}\Delta\rho_{\delta c}(T) = &\int_0^T dt_1\int_0^{t_1} dt_2\Phi_{\delta c}(t_1 - t_2)\\ &\times\frac{1}{2}\sigma_x\Omega_0(t_2)\rho_z(0)\cos[\vartheta(t_1)],\end{aligned}$$

where $\Phi_{\delta c}(t_1 - t_2) = \langle\delta(t_1)n_c(t_2)\rangle\Theta(t_1 - t_2)$ is the time correlation function, defined with the Heaviside function $\Theta(t_1 - t_2)$. Notice that in order to obtain this we ignored the $\sin(\cdots)$, constraining ourselves to π_x pulses.

We define $\Xi(t) = \cos[\vartheta(t)]\Theta(t)\Theta(T - t)$, and identify a convolution integral between the functions $\Phi_{\delta c}(t)$ and $\Omega_0(t)$, to write

$$\Delta\rho_{\delta c}(T) = \frac{1}{2}\sigma_x\rho_z(0)\int_0^T dt_1\,\Xi(t_1)[\Phi_{\delta c}(t_1) * \Omega_0(t_1)]. \tag{A6}$$

With the Fourier transform of the correlator (defined with a factor of 2 to compensate for the integration over half of the real axis), $G_{\delta c}(f) = 2\int_{-\infty}^{\infty} d\tau\, e^{-2\pi i f\tau}\Phi_{\delta c}(\tau)$ and a tilde ($\tilde{}$) to represent the Fourier transform of the other functions, $\Delta\rho_{\delta c}(T)$ can be written as

$$\begin{aligned}\Delta\rho_{\delta c}(T) &= \frac{1}{2}\sigma_x\rho_z(0)\int_0^T dt_1\,\Xi(t_1)\Phi_{\delta c}(t_1) * \Omega_0(t_1)\\ &= \frac{1}{4}\sigma_x\rho_z(0)\int_{-\infty}^{\infty} dt_1\,\Xi(t_1)\end{aligned}$$

$$\times \int_{-\infty}^{\infty} df_1 e^{2\pi i f_1 t_1} G_{\delta c}(f_1)\tilde{\Omega}_0(f_1)$$
$$= \frac{1}{4}\sigma_x\rho_z(0)\int_{-\infty}^{\infty} dt \int_{-\infty}^{\infty} df_2\, e^{2\pi i f_2 t}\,\tilde{\Xi}(f_2)$$
$$\times \int_{-\infty}^{\infty} df_1 e^{2\pi i f_1 t} G_{\delta c}(f_1)\tilde{\Omega}_0(f_1)$$
$$= \frac{1}{4}\sigma_x\rho_z(0)\int_{-\infty}^{\infty} df\ \tilde{\Xi}^*(f)\tilde{\Omega}_0(f)G_{\delta c}(f).$$

Defining $F_{\delta c}(f) = \tilde{\Xi}^*(f)\tilde{\Omega}_0(f)$, the change of the density matrix is compactly expressed by

$$\Delta\rho_{\delta c}(T) = \frac{1}{4}\sigma_x\rho_z(0)\int_{-\infty}^{\infty} df\ G_{\delta c}(f)F_{\delta c}(f). \tag{A7}$$

Similarly, repeating this procedure with the the other cross-correlation term in Eq. (A6), we obtain

$$\Delta\rho_{c\delta}(T) = \frac{1}{4}\sigma_z\rho_x(0)\int_{-\infty}^{\infty} df\ G_{c\delta}(f)F_{\delta c}(f), \tag{A8}$$

with $G_{c\delta}(f)$ defined the same as $G_{\delta c}(f)$ up to exchanging the functions $\delta(t)$ and $n_c(t)$. The other two terms are written explicitly in the main text (the environment overlap integral is derived in details in several previous works; see Ref. [14] for example).

This formalism can be generalized further to include frequency noise of the control, multiple axes control sequences, and other models of the control noise. In what follows, we give an outline for this possible expansion. Frequency (and phase) noise of the control are treated the same as the energy fluctuations $\delta(t)$. To see this, one has to change to the interaction picture which rotates with the frequency of the control local oscillator, including its classical frequency noise. In this interaction picture, the noise in the control is an additional σ_z noise (up to a minus sign) added to $\delta(t)$.

Multiple axes control sequences (π_x combined with π_y) should be considered carefully. Although changing the pulse axis is equivalent to a phase shift, it cannot be regarded as energy fluctuations like in the case of frequency noise of the control. Doing so is wrong since the phase shift cannot be considered sufficiently small to keep the weak coupling assumption valid. Instead, one should carry out a similar derivation to the one shown above. Applying this procedure, the commutators in Eq. (A6) become somewhat more complicated to calculate since there are no closed-form expressions for $\tilde{S}_\delta(t)$ and $\tilde{S}_c(t)$ (σ_x and σ_y are noncommuting). Nevertheless, $\tilde{S}_\delta(t)$ and $\tilde{S}_c(t)$ can be calculated directly, by evaluating the effect of the pulses, sequentially. Since the evolution between the pulses can be calculated analytically, the resulting filter function can always be expressed as a split function, making it possible to calculate the overlap integrals for finite number of pulses. In the case of a continues control, the sine term we disregarded in the treatment should be taken into account like it was done in [14].

The model for the noise in the control, modeled by $\Omega(t) = \Omega_0(t)[1 + n_c(t)]$, can be considered as general first-order treatment of the noise. In this model the noise is gated (multiplied) by the function $\Omega_0(t)$. However, one can consider also the case of additive noise which is not gated by this function:

$$\Omega(t) = \Omega_0(t)[1 + n_c(t)] + b(t). \tag{A9}$$

This is the case if the control is derived from an oscillator which is controlled by a noisy analog gate. However, the effect of this noise, $b(t)$, has the same effect as $n_c(t)$, but gated with a function which is constant during the entire experiment time, T. To regard this in our treatment the filter function must be replaced by

$$F_c(f) = \left|\int_0^T dt\, e^{-2\pi i f t}\right|^2, \tag{A10}$$

which is just the original filter function plugging $\Omega_0 = 1$. For the case in which the two kind of noises appear simultaneously, one should add an additional overlap integral [or two additional overlap integrals in case that the noises $b(t)$ and $n_c(t)$ are correlated].

2. Shot-to-shot fluctuations and the system density operator

The evolution of the density matrix, described by our framework, can be related directly to shot-to-shot fluctuations of the experimental results. For example, a strong noise in the control field can completely randomize the final state of the system. Consequently, the parameters ρ_x, ρ_y, and ρ_z, which parametrize the density operator, must be zero, for this randomized state. Similarly, measuring the shot-to-shot fluctuations, one can calculate the average parameters: ρ_x, ρ_y, and ρ_z. It is important to note that unlike the σ_z noise, the random effect of the control noise does not average out on the ensemble since all atoms are subjected to the same noise in a single realization. Therefore, the experiment must be repeated more than once in order to obtain the parameters ρ_x, ρ_y, and ρ_z.

The fluctuations of the density operator, are related to the average change in the density operator. This relation is captured by a geometrical interpretation of summing random vectors: The sum of random vectors, pointing at random directions, has a smaller magnitude than the sum of all vector lengths. Describing the density operator by a vector and applying this argument, one can derive the relation between its mean value and fluctuations. However, here we derive it similarly to the previous section, starting from the evolution of the density operator. The master equation for the density operator up to the first-order in the control noise is

$$\dot{\tilde{\rho}}_c(t) = \frac{1}{i\hbar}\left[\tilde{H}_{\rm int}(t),\, \tilde{\rho}(t)\right]. \tag{A11}$$

Plugging the interaction Hamiltonian, integrating over the short time T, and taking the trace to find the y-component of the vector, we obtain

$$\Delta\rho_y(T) = \mathrm{Tr}\{\Delta\rho_c(T)\sigma_y\}$$
$$= \mathrm{Tr}\left\{\frac{1}{i\hbar}\int_0^T dt\, n_c(t)[S_c(t),\rho(t)]\sigma_y\right\}$$
$$= \int_0^T dt\, n_c(t)\rho_z\Omega_0(t). \tag{A12}$$

Taking the expectation value of $\Delta\rho_y(T)$ yields zero as the noise $n_c(t)$ averages to zero. However, the fluctuations in this

component are readily calculated by

$$\langle(\Delta\rho_y(T))^2\rangle = \left\langle \int_0^T dt_1\, n_c(t_1)\rho_z\Omega_0(t_1) \int_0^T dt_2\, n_c(t_2)\rho_z\Omega_0(t_2)\right\rangle,$$

which in the frequency domain is written as

$$\langle(\Delta\rho_y(T))^2\rangle = \rho_z^2 \int_{-\infty}^{\infty} df\, G_c(f)F_c(f), \tag{A13}$$

where the density operator change, $\Delta\rho_y(T)$, can be replaced by the component $\rho_y(T)$ itself in this expression, since the initial density operator is not fluctuating.

3. Short-times fidelity

The fidelity $\mathcal{F} = \mathrm{Tr}\{\rho(t)\rho(0)\}$ is derived for short times for an initial pure state. For pure dephasing, it is written by

$$\mathcal{F} = \mathrm{Tr}\{\rho(t)\rho(0)\} = \mathrm{Tr}\{[\rho(0) + \Delta\rho(T)]\rho(0)\}.$$

Since $\rho(0)$ is a pure state, the trace of $\rho^2(0)$ is 1, and therefore

$$\begin{aligned}\mathcal{F} &= 1 + \mathrm{Tr}\{\Delta\rho(T)\rho(0)\}\\ &= 1 + \mathrm{Tr}\left\{\left(-\frac{\rho_x\sigma_x + \rho_y\sigma_y}{2}\frac{T}{2T}\int_{-\infty}^{\infty} df\, G_\delta(f)F_\delta(f)\right)\right.\\ &\quad\left.\times\frac{1}{2}(\rho_x\sigma_x + \rho_y\sigma_y + \rho_z\sigma_z + \mathbf{1})\right\}\\ &= 1 - \frac{1}{4}\mathrm{Tr}\{\sigma_x^2\}\rho_x^2\frac{T}{2T}\int_{-\infty}^{\infty} df\, G_\delta(f)F_\delta(f)\\ &\quad - \frac{1}{4}\mathrm{Tr}\{\sigma_y^2\}\rho_y^2\frac{T}{2T}\int_{-\infty}^{\infty} df\, G_\delta(f)F_\delta(f)\\ &= 1 - \frac{\rho_x^2}{4}\int_{-\infty}^{\infty} df\, G_\delta(f)F_\delta(f) - \frac{\rho_y^2}{4}\int_{-\infty}^{\infty} df\, G_\delta(f)F_\delta(f).\end{aligned} \tag{A14}$$

Using the same arithmetic with the noise in the control, one gets the fidelity of the system subjected to the two noises. It is written as

$$\mathcal{F} = 1 - \frac{\rho_x^2 + \rho_y^2}{2}TR_\delta(T) - \frac{\rho_y^2 + \rho_z^2}{2}TR_c(T), \tag{A15}$$

with the definitions for the decay rate functions

$$R_\delta(T) = \frac{1}{2T}\int_{-\infty}^{\infty} df\, G_\delta(f)F_\delta(f), \tag{A16}$$

and

$$R_c(T) = \frac{1}{2T}\int_{-\infty}^{\infty} df\, G_c(f)F_c(f). \tag{A17}$$

The definitions of $R_\delta(T)$ and $R_c(T)$ are useful since the functions are almost time independent for periodic pulses. This is due to the scaling of the filter function canceling the $1/T$ dependence. Hence the fidelity decays in a constant rate. It also helpful to note that the integral of the filter function $F_\delta(f)$ is just T and theretofore does not depend on the pulse frequency, but only on the total experiment time. However, the filter function $F_c(f)$ scales linearly with the pulse rate. Hence, the decay rate of the fidelity is large for spectral features at higher frequencies which is consistent with the experimental results.

[1] M. A. Nielsen and I. L. Chuang, *Quantum Computation and Quantum Information* (Cambridge University Press, Cambridge, 2000).
[2] M. H. Levitt, *Spin Dynamics: Basics of Nuclear Magnetic Resonance* (Wiley-Blackwell, New York, 2008).
[3] S. Kotler *et al.*, Nature (London) **473**, 61 (2011).
[4] Y. Sagi, I. Almog, and N. Davidson, Phys. Rev. Lett. **105**, 053201 (2010).
[5] L. Viola, S. Lloyd, and E. Knill, Phys. Rev. Lett. **83**, 4888 (1999).
[6] L. Viola, E. Knill, and S. Lloyd, Phys. Rev. Lett. **82**, 2417 (1999).
[7] C. Search and P. R. Berman, Phys. Rev. Lett. **85**, 2272 (2000).
[8] K. Khodjasteh and D. A. Lidar, Phys. Rev. Lett. **95**, 180501 (2005).
[9] G. S. Uhrig, Phys. Rev. Lett. **98**, 100504 (2007).
[10] J. Bylander *et al.*, Nat. Phys. **7**, 565 (2011).
[11] A. G. Kofman and G. Kurizki, Phys. Rev. Lett. **87**, 270405 (2001).
[12] G. Gordon, N. Erez, and G. Kurizki, J. Phys. B **40**, S75 (2007).
[13] H. Uys, M. J. Biercuk, and J. J. Bollinger, Phys. Rev. Lett. **103**, 040501 (2009).
[14] I. Almog *et al.*, J. Phys. B **44**, 154006 (2011).
[15] G. A. Alvarez and D. Suter, Phys. Rev. Lett. **107**, 230501 (2011).
[16] T. Green, H. Uys, and M. J. Biercuk, Phys. Rev. Lett. **109**, 020501 (2012).
[17] J. Clausen, G. Bensky, and G. Kurizki, Phys. Rev. Lett. **104**, 040401 (2010).
[18] K. C. Young and K. B. Whaley, Phys. Rev. A **86**, 012314 (2012).
[19] J. Avron, O. Kenneth, A. Retzker, and M. Shalyt, New J. Phys. **17**, 043009 (2015).
[20] L. Viola and E. Knill, Phys. Rev. Lett. **90**, 037901 (2003).
[21] A. M. Tyryshkin *et al.*, arXiv:1011.1903.
[22] A. M. Souza, G. A. Álvarez, and D. Suter, Phys. Rev. Lett. **106**, 240501 (2011).
[23] S. Cai *et al.*, New J. Phys. **14**, 113023 (2012).
[24] E. Magesan *et al.*, Phys. Rev. Lett. **109**, 080505 (2012).
[25] S. Pasini, P. Karbach, and G. S. Uhrig, Europhys. Lett. **96**, 10003 (2011).
[26] C. Stihl *et al.*, arXiv:1210.4311.
[27] K. Khodjasteh *et al.*, Nat. Commun. **4**, 2045 (2013).
[28] T. J. Green, J. Sastrawan, H. Uys, and M. J. Biercuk, New J. Phys. **15**, 095004 (2013).
[29] Y. Sagi, I. Almog, and N. Davidson, Phys. Rev. Lett. **105**, 093001 (2010).
[30] D. M. Harber, H. J. Lewandowski, J. M. McGuirk, and E. A. Cornell, Phys. Rev. A **66**, 053616 (2002).
[31] H. Y. Carr and E. M. Purcell, Phys. Rev. **94**, 630 (1954).
[32] S. Meiboom and D. Gill, Rev. Sci. Instrum. **29**, 688 (1958).
[33] T. A. Savard, K. M. O'Hara, and J. E. Thomas, Phys. Rev. A **56**, R1095 (1997).
[34] N. Navon, S. Kotler, N. Akerman, Y. Glickman, I. Almog, and R. Ozeri, Phys. Rev. Lett. **111**, 073001 (2013).